Calculation of Earth's Geomagnetic Field by Quantum Gravity Theory with Ultimate Acceleration

Huaiyang Cui
Department of Physics, Beihang University, Beijing, 102206, China
Email: hycui@buaa.edu.cn
(October 18 2023, submitted to viXra)

Abstract: In analogy with the ultimate speed c, there is an ultimate acceleration β, nobody's acceleration can exceed this limit β, in the solar system, β=2.956391e+10(m/s^2). Because this ultimate acceleration is a large number, any effect connecting to β will become easy to test, including quantum gravity tests. In this paper, an approach is put forward to connect the ultimate acceleration with quantum theory. As an application, the quantum gravity theory with the ultimate acceleration provides a mechanism to explain and calculate the geomagnetic field, the earth's geomagnetic field is calculated to be -0.6Gauss at the north pole.

1. Introduction

Some quantum gravity proposals [1,2] are extremely hard to test in practice, as quantum gravitational effects are appreciable only at the Planck scale [3]. But ultimate acceleration provides another scheme to deal with quantum gravity effects.

In analogy with the ultimate speed c, there is an ultimate acceleration β, nobody's acceleration can exceed this limit β, in the solar system, β=2.956391e+10(m/s^2). Because this ultimate acceleration is a large number, any effect connecting to β will become easy to test, including quantum gravity tests.

In recent years, de Broglie matter wave has been generalized in terms of the ultimate acceleration. Consider a particle, its relativistic matter wave is given by the path integral

$$\psi = \exp(\frac{i\beta}{c^3}\int_0^x (u_1 dx_1 + u_2 dx_2 + u_3 dx_3 + u_4 dx_4)) \quad . \tag{1}$$

where u is the 4-velocity of the particle, β is the ultimate acceleration determined by experiments. The β replaces the *Planck constant* in this quantum gravity theory so that *its wavelength becomes a length on planetary-scale*. The author's early paper shows that this generalized matter wave can explain the solar quantum gravity effects correctly, such as sunspot cycle, atmospheric circulation and human lifespan [21]. The present paper shows that this quantum gravity theory with the ultimate acceleration provides a mechanism to explain and calculate the geomagnetic field.

2. Extracting ultimate acceleration from the solar system

In the orbital model as shown in Fig.1(a), the orbital circumference is n multiple of the wavelength of the planetary-scale relativistic matter wave, according to Eq. (1), consider a

planet, we have

$$\left.\begin{aligned}\frac{\beta}{c^3}\oint_L v_l dl = 2\pi n \\ v_l = \sqrt{\frac{GM}{r}}\end{aligned}\right\} \Rightarrow \quad \sqrt{r} = \frac{c^3}{\beta\sqrt{GM}} n; \quad n = 0,1,2,\ldots \ . \tag{2}$$

This orbital quantization rule only achieves a half success in the solar system, as shown in Fig.1(b), the Sun, Mercury, Venus, Earth and Mars satisfy the quantization equation; while other outer planets fail. But, since we only study quantum gravity effects among the Sun, Mercury, Venus, Earth and Mars, so this orbital quantization rule is good enough as a foundational quantum theory. In Fig.1(b), the blue straight line expresses a linear regression relation among the quantized orbits, so it gives β=2.956391e+10 (m/s^2) by fitting the line. The quantum numbers n=3,4,5,... were assigned to the solar planets, the sun was assigned a quantum number n=0 because the sun is in the **central state**.

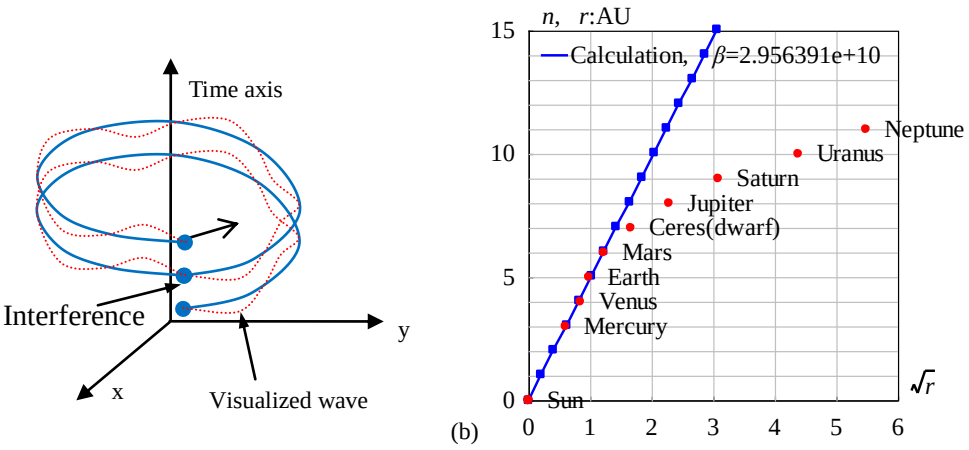

Fig.1 (a)The head of the relativistic matter wave may overlap with its tail. (b) The inner planets are quantized.

In the solar interior, if the coherent length of the relativistic matter wave is long enough, its head may overlap with its tail when the particle moves in a closed orbit, as shown in Fig.1(a). Consider a point on the solar equatorial plane, the overlapped wave is given by

$$\begin{aligned}&\psi = \psi(r)T(t)\\ &\psi(r) = 1 + e^{i\delta} + e^{i2\delta} + \ldots + e^{i(N-1)\delta} = \frac{1-\exp(iN\delta)}{1-\exp(i\delta)} \ .\\ &\delta(r) = \frac{\beta}{c^3}\oint_L (v_l)dl = \frac{2\pi\beta\omega r^2}{c^3}\end{aligned} \tag{3}$$

where N is the overlapping number which is determined by the coherent length of the relativistic matter wave, δ is the phase difference after one orbital motion, ω is the angular speed of the solar rotation. The above equation is a multi-slit interference formula in optics, for a larger N it becomes the Fabry-Perot interference.

The relativistic matter wave function ψ needs a further explanation. In quantum mechanics, $|\psi|^2$ equals to the probability of finding an electron due to Max Born's explanation; in astrophysics, $|\psi|^2$ equals to the probability of finding a nucleon (proton or neutron) *averagely on an astronomic scale*, we have

$$|\psi|^2 \propto \text{nucleon-density} \propto \rho \quad . \tag{4}$$

It follows from the multi-slit interference formula that the overlapping number N is estimated by

$$N^2 = \frac{|\psi(0)_{multi-wavelet}|^2}{|\psi(0)_{one-wavelet}|^2} = \frac{\rho_{core}}{\rho_{surface\_gas}} \quad . \tag{5}$$

The solar core has a mean density of 1408 (kg/m^3), the surface of the sun is comprised of convective zone with a mean density of 2e-3 (kg/m^3) [7]. In this paper, the sun's radius is chosen at a location where density is 4e-3 (kg/m^3), thus the solar overlapping number N is calculated to be N=593. Since the mass density $\rho(r)$ has approximately spherical symmetry, then the $\psi(r)$ has the spherical symmetry.

Sun's angular speed at its equator is known as ω=2π/(25.05x24x3600) (s^{-1}). Its mass 1.9891e+30 (kg), the well-known radius 6.95e+8 (m), the mean density 1408 (kg/m^3), the constant β=2.956391e+10 (m/s^2). According to the N=593, the matter distribution of the $|\psi|^2$ is calculated in Fig.2(a), it agrees well with the general description of star's interior. The radius of the sun is determined as r=7e+8 (m) with a relative error of 0.72% in Fig.2, which indicates that the sun radius strongly depends on the sun's self-rotation.

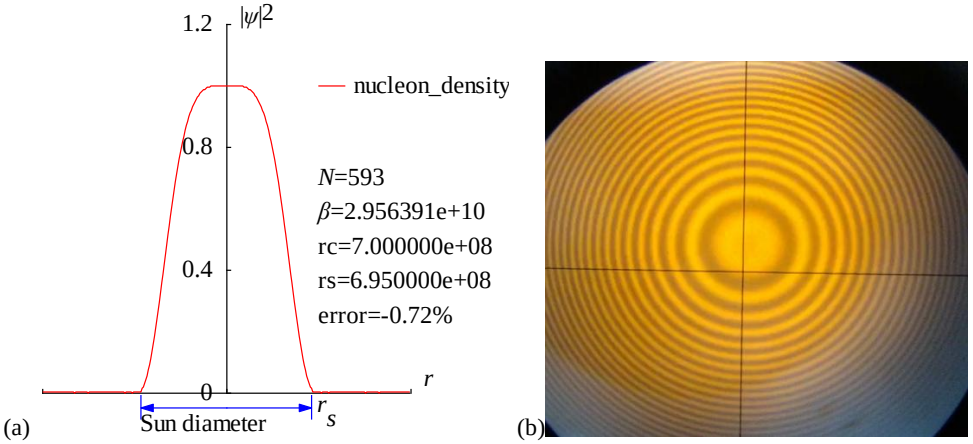

Fig.2 (a)The nucleon distribution $|\psi|^2$ in the Sun is calculated in the radius direction. (b) As contrast, sodium Fabry-Perot interference (δ=const.).

```
<Clet2020 Script>//C source code [17]
int i,j,k,m,n,N,nP[10];
double beta,H,B,M,r,r_unit,x,y,z,delta,D[1000],S[1000], a,b,rs,rc,omega,atm_height; char str[100];
main(){k=150;rs=6.95e8;rc=0;x=25.05;omega=2*PI/(x*24*3600);n=0; a=1408/0.004; N=sqrt(a);
beta=2.956391e10;H=SPEEDC*SPEEDC*SPEEDC/beta;M=1.9891E30; atm_height=2e6; r_unit=1E7;
for(i=-k;i<k;i+=1) {r=abs(i)*r_unit;
if(r<rs+atm_height) delta=2*PI*omega*r*r/H; else delta=2*PI*sqrt(GRAVITYC*M*r)/H;//around the star
x=1;y=0; for(j=1;j<N;j+=1) { z=delta*j; x+=cos(z);y+=sin(z);} z=x*x+y*y; z=z/(N*N);
S[n]=i;S[n+1]=z; if(i>0 && rc==0 && z<0.0001) rc=r; n+=2;}
SetAxis(X_AXIS,-k,0,k,"#ifr; ; ; ");SetAxis(Y_AXIS,0,0,1.2,"#if|ψ|#su2#t;0;0.4;0.8;1.2;");
DrawFrame(FRAME_SCALE,1,0xafffaf); z=100*(rs-rc)/rs;
SetPen(1,0xff0000);Polyline(k+k,S,k/2,1," nucleon_density"); SetPen(1,0x0000ff);
r=rs/r_unit;y=-0.05;D[0]=-r;D[1]=y;D[2]=r;D[3]=y; Draw("ARROW,3,2,XY,10,100,10,10,",D);
Format(str,"#ifN#t=%d#n#ifβ#t=%e#nrc=%e#nrs=%e#nerror=%.2f%",N,beta,rc,rs,z);
TextHang(k/2,0.7,0,str);TextHang(r+5,y/2,0,"#ifr#sds#t");TextHang(-r,y+y,0,"Sun diameter");
}#v07=?>A
```

3. Extracting ultimate acceleration from the earth

Appling the planetary-scale relativistic matter wave to the Moon, as illustrated in Fig.3, The

moon is assigned a quantum number of n=2 because some quasi-satellite's perigees have reached a depth almost at n=1 orbit, as shown in Fig.3. Here, the ultimate acceleration β=1.377075e+14(m/s^2) is determined uniquely by the line between the earth and moon in Fig.3 by Eq. (2).

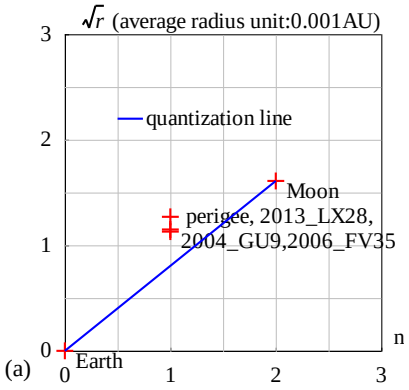

Fig.3 Orbital quantization for the moon.

```
<Clet2020 Script>// C source code [17]
char str[200];int i,j,k,N,nP[10]; double x,y,z,M,r_unit,a,b,B,H,r_ave[20],dP[10],D[1000];
double orbit[10]={0,2.57,0,}; double e[10]={0, 0.0549,0,0,0,0,0,0,0,0,};
int qn[10]={0,2,3,4,5,6,7,8,9.,10,};
char Stars[100]={"Earth;Moon;"};
int main(){ N=2; M=5.97237E24; r_unit=1.495978707e8;
for(i=0;i<N;i+=1) {x=orbit[i];y=e[i]; z=x*(1+sqrt(1-y*y))/2;r_ave[i]=z;//average_radius
D[i+i]=qn[i];D[i+i+1]=sqrt(z); }
DataJob("REGRESSION,2",D,dP);b=dP[0];a=dP[1];
SetAxis(X_AXIS,0,0,3,"n;0;1;2;3;");
SetAxis(Y_AXIS,0,0,3," #if#rsr#t (average radius unit:0.001AU);0;1;2;3;");
DrawFrame(0x0166,1,0xafffaf); Polyline(N,D);
SetPen(2,0xff0000); Plot("OVALFILL,0,2,XY,3,3,",D);
for(i=0;i<N;i+=1) {nP[0]=TAKE;nP[1]=i;TextJob(nP,Stars,str);x=qn[i]+0.2;
y=sqrt(orbit[i])-0.05;TextHang(x,y,0,str);}
x=GRAVITYC*M*r_unit;z=sqrt(x);H=z*a;B=-z*b;
TextAt(100,450,"#ifH#t=%e    #ifB#t=%e",H,B);
for(i=0;i<N;i+=1) {y=b+a*qn[i];D[i+i]=qn[i];D[i+i+1]=y;}
SetPen(1,0x0000ff);Polyline(N,D,0.5,2.2,"quantization");//check
}}#v07=?>A#t
```

Now let us talk about the earth's interior, the earth has a mean density of 5530 (kg/m^3), its surface is covered with air and vapor with a density of 1.29 (kg/m^3). The earth's radius is chosen at the sea level, it follows Eq.(5) that the earth's overlapping number N is calculated to be N=65.

The earth's angular speed is known as ω=2π/(24x3600) (s^{-1}), its mass 5.97237e+24 (kg), the well-known radius is 6.378e+6 (m), the earth's constant β=1.377075e+14 (m/s^2). The matter distribution $|\psi|^2$ in radius direction is calculated by Eq.(3), as shown in Fig.4(a). The radius of the earth is determined as r=6.4328e+6 (m) with a relative error of 0.86%, it agrees well with common knowledge. Space debris over the atmosphere has a complicated evolution [9,10], has itself speed

$$v_l=\sqrt{\frac{GM}{r}};\quad \delta(r)=\frac{\beta}{c^3}\oint_L(v_l)dl=\frac{2\pi\beta}{c^3}\sqrt{GMr}\quad . \tag{6}$$

The secondary peaks over the atmosphere up to 2000km altitude are calculated out in Fig.4(b) which agrees well with the space debris observations [9]; the peak near 890 km altitude is due principally to the January 2007 intentional destruction of the Fengyun-1C weather spacecraft, while the peak centered at approximately 770 km altitude was created by the February 2009 accidental collision of Iridium 33 (active) and Cosmos 2251 (derelict) communication

spacecraft [9,10,11]. The observations based on the incoherent scattering radar EISCAT ESR located at 78 ℕ in Jul. 2006 and in Oct. 2015 [12,13,14] are respectively shown in Fig.4(c) and (d). This prediction to secondary peaks also agrees well with other space debris observations [15,16].

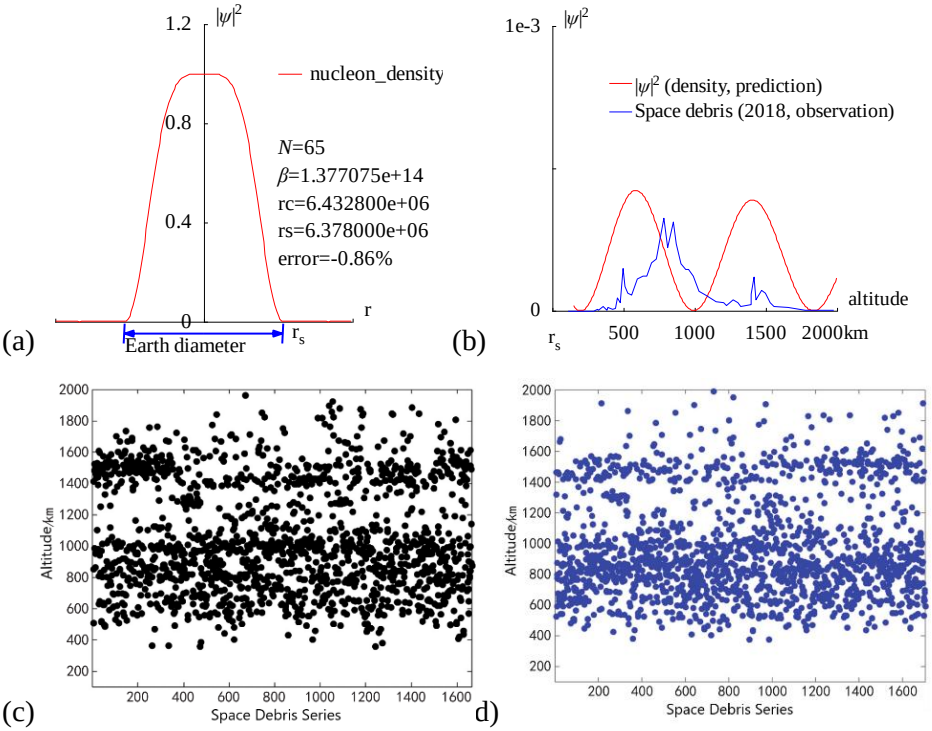

Fig.4 (a) The radius of the Earth is calculated out r=6.4328e+6 (m) with a relative error 0.86% by the interference of its acceleration-roll wave; (b) The prediction of the space debris distribution up to 2000km altitude; (c) The pace debris distribution in Jul. 2006, Joint observation based on the incoherent scattering radar EISCAT ESR located at 78 ℕ [12]; (d) The space debris distribution in Oct. 2015, Joint observation based on the incoherent scattering radar EISCAT ESR located at 78 ℕ [12].

```
<Clet2020 Script>//C source code [17]
int i,j,k,m,n,N,nP[10]; double H,B,M,v_r,r,AU,r_unit,x,y,z,delta,D[10],S[1000];
double rs,rc,rot,a,b,atm_height,beta; char str[100];
main(){k=80;rs=6.378e6;rc=0;atm_height=1.5e5;n=0; N=65;
beta=1.377075e+14;H=SPEEDC*SPEEDC*SPEEDC/beta;
M=5.97237e24;AU=1.496E11;r_unit=1e-6*AU; rot=2*PI/(24*60*60);//angular speed of the Earth
for(i=-k;i<k;i+=1) {r=abs(i)*r_unit;
if(r<rs+atm_height) v_r=rot*r*r; else v_r=sqrt(GRAVITYC*M*r);//around the Earth
delta=2*PI* v_r/H; y=SumJob("SLIT_ADD,@N,@delta",D); y=y/(N*N);
if(y>1) y=1; S[n]=i;S[n+1]=y; if(i>0 && rc==0 && y<0.001) rc=r;    n+=2;}
SetAxis(X_AXIS,-k,0,k,"r; ; ; ;");SetAxis(Y_AXIS,0,0,1.2,"#if|ψ|#su2#t;0;0.4;0.8;1.2;");
DrawFrame(FRAME_SCALE,1,0xafffaf); x=50;z=100*(rs-rc)/rs;
SetPen(1,0xff0000);Polyline(k+k,S,k/2,1," nucleon_density");
r=rs/r_unit;y=-0.05;D[0]=-r;D[1]=y;D[2]=r;D[3]=y;
SetPen(2,0x0000ff); Draw("ARROW,3,2,XY,10,100,10,10,",D);
Format(str,"#ifN#t=%d#n#if β#t=%e#nrc=%e#nrs=%e#nerror=%.2f%",N,beta,rc,rs,z);
TextHang(k/2,0.7,0,str);TextHang(r+5,y/2,0,"r#sds#t");TextHang(-r,y+y,0,"Earth diameter");
}#v07=?>A#t
<Clet2020 Script>//C source code [9]
int i,j,k,m,n,N,nP[10]; double H,B,M,v_r,r,AU,r_unit,x,y,z,delta,D[10],S[10000];
double rs,rc,rot,a,b,atm_height,p,T,R1,R2,R3; char str[100]; int
Debris[96]={110,0,237,0,287,0,317,2,320,1,357,5,380,1,387,4,420,2,440,3,454,14,474,9,497,45,507,26,527,19,557,17,597,34,63
4,37,664,37,697,51,727,55,781,98,808,67,851,94,871,71,901,50,938,44,958,44,991,37,1028,21,1078,17,1148,10,1202,9,1225,6,
1268,12,1302,9,1325,5,1395,7,1395,18,1415,36,1429,12,1469,22,1499,19,1529,9,1559,5,1656,4,1779,1,1976,1,};
main(){k=80;rs=6.378e6;rc=0;atm_height=1.5e5;n=0; N=65;
H=1.956611e11;M=5.97237e24;AU=1.496E11;r_unit=1e4;
rot=2*PI/(24*60*60);//angular speed of the Earth
b=PI/(2*PI*rot*rs*rs/H); R1=rs/r_unit;R2=(rs+atm_height)/r_unit;R3=(rs+2e6)/r_unit;
for(i=R2;i<R3;i+=1) {r=abs(i)*r_unit; delta=2*PI*sqrt(GRAVITYC*M*r)/H;
y=SumJob("SLIT_ADD,@N,@delta",D); y=1e3*y/(N*N);// visualization scale:1000
if(y>1) y=1; S[n]=i;S[n+1]=y;n+=2;}
SetAxis(X_AXIS,R1,R1,R3,"altitude; r#sds#t;500;1000;1500;2000km ;");
SetAxis(Y_AXIS,0,0,1,"#if|ψ|#su2#t;0; ;1e-3;");DrawFrame(FRAME_SCALE,1,0xafffaf); x=R1+(R3-R1)/5;
SetPen(1,0xff0000);Polyline(n/2,S,x,0.8,"#if|ψ|#su2#t (density, prediction)");
```

for(i=0;i<48;i+=1) {S[i+i]=R1+(R3-R1)*Debris[i+i]/2000; S[i+i+1]=Debris[i+i+1]/300;}
SetPen(1,0x0000ff);Polyline(48,S,x,0.7,"Space debris (2018, observation) "); }#v07=?>A#t

4. Stellar rotation under the control of relativistic matter waves

As shown in Fig.5(a), the sun at the origin of the planetary plane x-y, a typical relativistic matter wave $\psi(r)$ in the r-direction is given in terms of the cylinder coordinates (r,φ,z) by

$$\psi(r,t)=\frac{1}{\sqrt{r}}\sin(kr-\omega t) \quad . \tag{7}$$

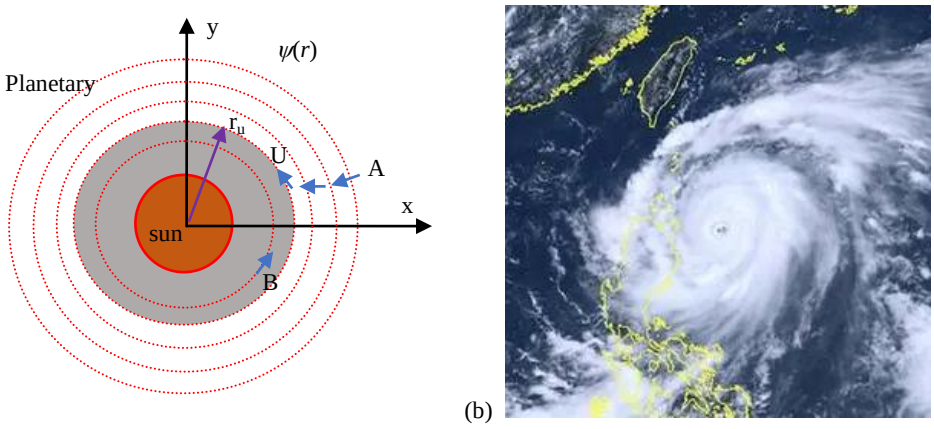

Fig.5 (a) The direction of the wave-vector ***k*** varies as the radius changes from A to U. (b) Tropic vortex (Doksuri, July 26 2023, 10AM) forms on the Pacific ocean, China FY-4B satellite photo.

where we have used ***k*** to denote the wave-vector, $k=2\pi/\lambda$. In the 2D plane, the r-component of the matter wave is governed by the Bessel equation

$$\frac{d^2\psi}{dr^2}+(k^2-\frac{1}{4r^2})\psi=0 \quad . \tag{8}$$

Readers can check its validity by simply substituting ψ into the Bessel equation. It indicates that the direction of the wave-vector ***k*** varies as the radius changes while the wavelength is invariant, that is

$$k^2=k_r{}^2+k_\varphi{}^2; \quad k_r{}^2=k^2-\frac{1}{4r^2}; \quad k_\varphi=\pm\frac{1}{2r} \quad . \tag{9}$$

Considering a converging wave, from the point A to the point U in Fig,5(a), the direction of the wave-vector ***k*** has changed from the almost r-direction to the almost φ-direction, the U point locates at the radius r_u where we find

$$k_r=0; \quad k_\varphi=\frac{1}{2r_u}=k \quad . \tag{10}$$

As shown in Fig.5(b), a tropic vortex (July 26 2023, FY=4B satellite photo) on the Pacific ocean forms with releasing its extra angular momentum $k_\varphi=1/2r$. We deduce that in the rang $r<r_u$ as indicated at the point B the wave-vector is

$$r < r_u: \quad k_r = 0; \quad k_\varphi = k \quad . \tag{11}$$

In the process from A to U, a molecule at A with thermal motion (v_r,x_φ,v_z) becomes a new-style motion at U: thermal motion (0,x_φ,v_z) + vortex flow (v_{flow}=v_r); in other words, the *r*-component of the thermal motion transforms gradually into the circular vortex flow during the process from A to U. In the range $r<r_u$, like the solar surface where $r<r_u$, the thermal motion of gas is characterized as the followings:

(1) The motion in the *r*-direction is forbidden on planetary-scale

As shown in Fig.5(a), at the point B, in this ideal model, the thermal motion of gas in the *r*-direction is depressed, instead by the circular vortex flow v_{flow} which is transformed from the *r*-component of the thermal motion according the knowledge of analyzing the process from A to U. Thus, according to the energy equipartition theorem, we have

$$v_\varphi = \sqrt{\frac{k_B T}{m}}; \quad v_z = \sqrt{\frac{k_B T}{m}}; \quad v_r \approx 0; \quad v_{flow} = \sqrt{\frac{k_B T}{m}}; \quad . \tag{12}$$

where, k_B is the Boltzmann constant. The above equations can be used to determine celestial surface temperatures by measuring circular vortex flows in the range $r<r_u$.

(2) Electron flow is faster than ion flow in a plasma vortex.

We have know that the energy of a circular vortex flow comes from the transformation of the *r*-component of thermal motion, since electron mass is less than ion mass in a plasma, the electron flow is faster than the ion flow in the plasma vortex at the same temperature:

$$v_{flow\_electron} = \sqrt{\frac{k_B T}{m_{electron}}} > v_{flow\_ion} = \sqrt{\frac{k_B T}{m_{ion}}} \quad . \tag{13}$$

The faster circular electron flow relative to the massive ion flow would produce a magnetic filed in the vortex, for example, sunspots are a typical vortex with a observable magnetic field.

(3) Compliance of the 2D model to realistic 3D situation

In practice, in one hand, this 2D plane model will often be applied to 3D situation which appears to comply with similar equations; in another hand, many circular quantum vortices may develop into different stages and would be regarded as mature or immature, therefore, we have to introduce a **compliance coefficient** ξ so that this temperature formula is modified as

$$T = \xi \frac{m v_{flow}^{\ 2}}{k_B} . \tag{14}$$

For a mature 2D vortex, its compliance coefficient ξ is 1; for a 3D immature situation, ξ <1.

(4) Left-hand vortex and right-hand vortex

In the outer rang $r>r_u$, the double-valued φ-component of the wave-vector represents the left-hand vortex or right-hand vortex.

$$k_\varphi = \pm \frac{1}{2r}; \quad r > r_u \quad . \tag{15}$$

In the inner rang $r<r_u$, the *r*-component of motion is forbidden on planetary-scale, if the molecules at point B in Fig.5(a) want to transform its emerging *r*-component of motion into

the circular vortex flow, they have to at once decide how to choose which one of the two branches (k_r=0, k_φ=±k); actually their choices comply with the existing majority during the transformation. The Bessel equation is a uncertainty generator with a choice-mechanism, the rang $r<r_u$ is confined by the uncertainty radius r_u. In practices, only one chirality appears for one vortex.

5. Earth's geomagnetic field

The earth radius is r_s=6378km with the angular speed $\omega=2\pi/(24*3600)$ (s^{-1}), the atoms on the earth's equator have the rotating speed $v=r_s\omega$=463m/s in the frame of reference of the earth's orbit. The uncertainty radius is estimated by

$$\begin{aligned} & r_u = \frac{1}{2k} = \frac{\lambda}{4\pi} = 2.1e+5(\text{km}) \\ & r_s << r_u \end{aligned} \quad . \tag{16}$$

All earth's body is in the rang $r<r_u$, within which any attempt of electrons or molecules to move in the r-direction is depressed on planetary-scale, instead by a way to transform their kinetic energies in the r-direction into circular vortex flows around the earth's center

$$v_\varphi = \sqrt{\frac{k_B T}{m}}; \quad v_z = \sqrt{\frac{k_B T}{m}}; \quad v_r \approx 0; \quad v_{flow} = \sqrt{\frac{k_B T}{m}}; \quad . \tag{17}$$

Since electron mass is less than ion mass in the earth's soil, electron flow in the soil would be faster than the soil. But in practice, these theoretical electron flows in the earth's soil are constantly destroyed by inelastic collisions among various thermal activities, actually it is not easy to get to measure the electron flows in the soil; nevertheless, there are some residual electron flows in the mantle of the earth, the evidence is that they produce a geomagnetic field for the earth. Therefore, a rational estimation to the residual electron flows is made to take at

$$v_{flow\_electron\_residual} \approx 2v_{flow\_rotating} = 2\omega r \, . \tag{18}$$

Nevertheless, the faster circular electron flows relative to the massive soil would produce a geomagnetic filed around the earth. The earth's temperature distribution is also under the control of relativistic matter waves, for this topic see Ref.[24].

Now let us calculate the earth's magnetic field B at the north pole. The earth's soil and rocks in the equatorial plane are rotating at the speed $v=r\omega$, Assume that the speed of residual electronic flow is given by $v_{flow\_electron\_residual}=2r\omega$, as shown in Fig.6(a).

The n_e denotes the conducting electron density, according to the magnetic field formula of a single coil, as shown in Fig.6(b), the B at the north pole is given by

$$\begin{aligned} & B = \int_{r=0}^{r=r_s} \int_{A=-\pi/2}^{A=\pi/2} -\frac{\mu_0 R^2 e n_e (v_e - \omega R) r dr dA}{2(R^2 + (r_s - r\sin A)^2)^{3/2}}; \quad R = r\cos A \\ & n_e = 8e+11(m^{-3}) \quad \Rightarrow \quad B = -0.62(Gauss) \end{aligned} \quad . \tag{19}$$

By fitting data, if the conducting electron density takes at n_e =8e+11(m^{-3}), then we obtain the earth's geomagnetic field at the north pole B=-0.62Gauss, which is consistent with

experimental observation. To note that the conducting electron density is very thin, about 1.3e-12(/mole). Mars and Venus are either too small to have a convective core or rotate very slowly, so they are with weak or no magnetic fields.

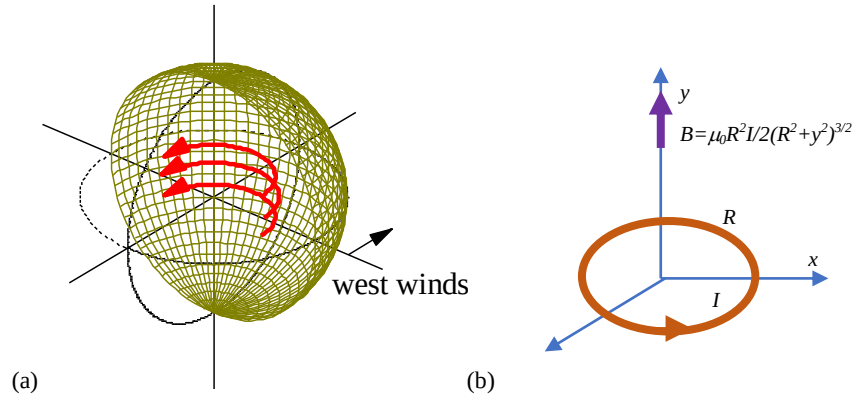

Fig.6 (a) The faster circular electron flows relative to the massive soil would produce a geomagnetic filed around the earth. (b) The magnetic field of a single coil.

```
<Clet2020 Script>// [17]
double dP[20],D[2000],r,v1,v2,K1,K2; int i,j,k,N;
int main(){ N=50; r=60; dP[0]=POLYLINE;dP[1]=0;dP[2]=N+1;dP[3]=XYZ;dP[4]=16;
SetViewAngle("temp0,theta60,phi-40");
DrawFrame(FRAME_LINE,1,0xafffaf);Overlook("2,1,60", D);
Draw("ARROW,0,2,XYZ,16","80,0,0,80,30,0"); TextHang(70,0,-20,"west winds");
SetPen(1,0xed9121); for(i=0;i<=180;i+=5) {k=0; K1=0; K2=i; Grid();}
for(i=0;i<=180;i+=5) {k=1; K1=i; K2=0; Grid();}
//TextAt(10,10,"v1=%d, v2=%d, T=%.2f y, λ=%e, V=%d",v1,v2,T, Lamda,V);
SetPen(3,0xff0000); k=1; K1=70; K2=0;r=30; dP[1]=3; Grid();
K1=90; K2=0;r=30; dP[1]=3; Grid(); K1=110; K2=0;r=30; dP[1]=3; Grid();
}
Grid(){ K1*=PI/180; K2*=PI/180; if(k==0) {v1=PI/N; v2=0;} else {v1=0; v2=PI/N;}
for(j=0;j<=N;j+=1){ k=j+j+j; D[k]=r*sin(K1)*cos(K2);D[k+1]=r*sin(K1)*sin(K2); D[k+2]=r*cos(K1);
K1+=v1;K2+=v2; }Plot(dP,D);
}#v07=?>A#t
```

```
<Clet2020 Script>// [17]
double beta,M,r,rc,rs,rot,ne,V,R,A,B,a,b,d,m,v1,v2,T,Year,K; int i,j,k;
int main(){beta=1.377075e+14; M=5.97237e24; rs=6.378e6;
rot=2*PI/(24*3600);    B=0; a=rs/100; b=PI/100; ne=8e11;
for(i=1;i<100;i+=1) { r=a*i; for(j=0;j<100;j+=1) { A=b*(j-50); R=r*cos(A); V=rot*R;
d=rs-r*sin(A); d=R*R+d*d; d=sqrt(d); d=2*d*d*d;
B+=MC*R*R*CHARGEC*ne*V*r/d; }}
B=B*a*b; m=ne/AVOGADRO; TextAt(100,100,"ne=%e,    m=%e, B=%e", ne, m, B);
v1=rot*rs; v2=0; K=SPEEDC*SPEEDC*SPEEDC/(2*beta*v1);
TextAt(100,200,"v1=%e, v2=%e, K=%e,",v1,v2,K);
}#v07=?>A
```

6. Conclusions

In analogy with the ultimate speed c, there is an ultimate acceleration β, nobody's acceleration can exceed this limit β, in the solar system, β=2.956391e+10(m/s^2). Because this ultimate acceleration is a large number, any effect connecting to β will become easy to test, including quantum gravity tests. In this paper, an approach is put forward to connect the ultimate acceleration with quantum theory. As an application, the quantum gravity theory with the ultimate acceleration provides a mechanism to explain and calculate the geomagnetic field, the earth's geomagnetic field is calculated to be -0.6Gauss at the north pole.

References

[1]C. Marletto, and V. Vedral, Gravitationally Induced Entanglement between Two Massive Particles is Sufficient Evidence of Quantum Effects in Gravity, Phys. Rev. Lett., 119, 240402 (2017)
[2]T. Guerreiro, Quantum effects in gravity waves, Classical and Quantum Gravity, 37 (2020) 155001 (13pp).
[3]S. Carlip, D. Chiou, W. Ni, R. Woodard, Quantum Gravity: A Brief History of Ideas and Some Prospects, International Journal of Modern Physics D, V,24,14,2015,1530028. DOI:10.1142/S0218271815300281.
[4]de Broglie, L., CRAS,175(1922):811-813, translated in 2012 by H. C. Shen in Selected works of de Broglie.
[5]de Broglie, Waves and quanta, Nature, 112, 2815(1923): 540.
[6]de Broglie, Recherches sur la théorie des Quanta, translated in 2004 by A. F. Kracklauer as De Broglie, Louis, On the Theory of Quanta. 1925.
[7]NASA, https://solarscience.msfc.nasa.gov/interior.shtml.
[8]NASA, https://nssdc.gsfc.nasa.gov/planetary/factsheet/marsfact.html.
[9]Orbital Debris Program Office, HISTORY OF ON-ORBIT SATELLITE FRAGMENTATIONS, National Aeronautics and Space Administration, 2018, 15 th Edition.
[10]Orbital Debris Program Office, Chinese Anti-satellite Test Creates Most Severe Orbital Debris Cloud in History, Orbital Debris Quarterly News, 2007, April,v11i2,
[11]D. Wright, Space debris, Physics today,2007,10,35-40.
[12]TANG Zhimei, DING Zonghua, DAI Liandong, WU Jian, XU Zhengwen, "The Statistics Analysis of Space Debris in Beam Parking Model in 78 °North Latitude Regions," Space Debris Research, 2017, 17,3, 1-7.
[13]TANG Zhimei DlNG, Zonghua, YANG Song, DAI Liandong, XU Zhengwen, WU Jian The statistics analysis 0f space debris in beam parking model based On the Arctic 500 MHz incoherent scattering radar, CHINESE JOURNAL 0F RADIO SCIENCE, 2018, 25,5, 537-542
[14]TANG Zhimei , DING, Zonghua , DAI Liandong , WU Jian , XU Zhengwen, Comparative analysis of space debris gaze detection based on the two incoherent scattering radars located at 69N and 78N, Chin . J . Space Sci, 2018 38,1, 73-78. DOI:10.11728/cjss2018.01.073
[15]DING Zong-hua, YANG Song, JIANG hai, DAI Lian-dong, TANG Zhi-mei, XU Zheng-wen, WU Jian, The Data Analysis of the Space Debris Observation by the Qujing Incoherent Scatter Radar, Space Debris Research, 2018, 18,1, 12-19.
[16]YANG Song, DING Zonghua, Xu Zhengwe, WU Jian, Statistical analysis on the space posture, distribution, and scattering characteristic of debris by incoherent scattering radar in Qujing, Chinese Journal of Radio science, 2018 33,6 648-654, DOI:10.13443/j.cjors.2017112301
[17]Clet Lab, Clet: a C compiler, download at https://drive.google.com/file/d/1OjKqANcgZ-9V5 6rgcoMtOu9w4rP49sgN/view?usp=sharing
[18]Huaiyang Cui, Relativistic Matter Wave and Its Explanation to Superconductivity: Based on the Equality Principle, Modern Physics, 10,3(2020)35-52. https://doi.org/10.12677/MP.2020.103005
[19]Huaiyang Cui, Relativistic Matter Wave and Quantum Computer, Amazon Kindle ebook, 2021.
[20]Huaiyang Cui, (2023) Determination of Solar Radius and Earth's Radius by Relativistic Matter Wave, Journal of Applied Mathematics and Physics, 11:1, DOI: 10.4236/jamp.2023.111006
[21]Huaiyang Cui, (2023) Biological Clock of Relativistic Matter Wave and Calculation of Human Mean Lifespan 84 Years, Modern Physics (in Chinese), 2023, 13(2): 28-41. DOI: 10.12677/mp.2023.132005; Huaiyang Cui, (2023) Modelling of Human Lifespan -- Based on Quantum Gravity Theory with Ultimate Acceleration, viXra:2302.0121. https://vixra.org/abs/2302.0121
[22]N.Cox, Allen's Astrophysical Quantities, Springer-Verlag, 2001, 4th ed..
[23] S. E. Schneider, T. T. Arny, Pathways to Astronomy, McGraw-Hill Education, 2018, 5th ed.
[24]Huaiyang Cui, (2023) Ultimate Acceleration in Quantum Mechanics to Explain and Calculate Earth's Geomagnetic Field: 0.6Gauss, viXra:2210.0140. https://vixra.org/abs/ 2210.0140